CHAPTER V
CATALYTIC PYROLYSIS OF WASTE TIRE
WITH NOBLE METALS-LOADED HMOR CATALYSTS

5.1 Abstract

The catalytic pyrolysis of waste tire with noble metals (Pt, Ru, Re, Rh) supported on HMOR catalysts was investigated. The pyrolysis results indicate an important increase in the yield of gaseous product at the expense of liquid yield when the bifunctional catalysts were introduced. Moreover, the contents of polycyclic and polar-aromatics decrease drastically for all prepared catalysts. As a consequence, the derived oils are much lighter and contain high concentration of saturates. Regarding the light oil production as well as aromatic reduction, the general catalytic activity order can be summarized as followed: Ru > Rh > Pt >> Re. Additionally, the catalytic activity under the studied conditions for the current catalysts does not depend on the metal dispersion as well as the total concentration of acid sites, but depends on the intrinsic nature of the metals themselves. The best performance of Ru catalyst was found to relate to its sulfur tolerance and coke resistance.

5.2 Introduction

The more stringent environmental regulations concerning the waste tire in recent years have favored the recycling alternatives of this waste instead of dumping in the open air or in the land-filled. Thus, tire pyrolysis, a recycling process, has attracted renewed significant attention. Tire pyrolysis essentially produces a carbonized char, condensable oil, and a gas fraction. The gas fraction has been reported to have a high calorific value [1], and high hydrogen content [2-4], whereas the tire-derived oil was shown to be similar, to a certain extent, to the commercial petroleum naphtha [5]. However, the high concentration of aromatic hydrocarbons (HCs) [5-7], especially polycyclic HCs (PAHs), has limited its application as a fuel since the high emissions of smoke, hydrocarbon (HC), and CO were reported when pyrolysis oil was used in an engine [8]. Our previous study [9] has shown that the

mordenite-catalyzed pyrolysis of waste tire produced the oil having high selectivity toward gasoline, kerosene, and gas oil fractions. However, a relatively high amount of polycyclic aromatics and polar-aromatics still existed in the oil.

Bifunctional catalysts with both metal and acid functions are extensively studied for the reduction of aromatics in fuels [10-13]. Metals can catalyze the hydrogenation of the feedstock, making it more reactive for cracking and heteroatoms (sulfur, oxygen) removal [11]. And a high level of aromatic hydrogenation at moderate hydrogen pressures can be achieved with noble metals catalysts [12,13]. The intrinsically high hydrogenation activity of noble metals might also help reducing steric effects that impede the direct elimination of the sulfur heteroatom [14,15]. However, noble metals display a low resistance to sulfur poisoning; thus, limiting their applications. The sulfur tolerance of a noble metal supported catalyst may be enhanced by (i) using acidic carriers [16], (ii) changing the metal particle size, or (iii) alloying with other metals [17]. Moreover, for noble metal supported on acid zeolite catalyst, the acid site can exhibit some hydrogenation activity due to the hydrogen spill-over effect [18]. Rh, Pt, and Ru-supported catalysts were reported to have high activity for aromatic hydrogenation [13,19,20]. Albertazzi et al. investigated the hydrogenation of naphthalene of various metals (Rh, Pd, Pt, Ru, Ir)-supported catalysts, and found that the catalytic activity of Rh and Pd-catalysts was higher than that of Ir, Ru, and Pt-based catalysts [20]. Although rhenium was shown to catalytically inactive in the hydroconversion [21], it has frequently been used as a promoter for Pt catalysts [22] and particularly as catalysts for the sulfur removal in the HDS reactions [23]. Thus, the catalytic behavior of Re/HMOR catalyst is also worth being investigated for the waste tire conversion.

The aim of this work is to investigate the catalytic activity of noble metals (Ru, Pt, Re, Rh) supported on HMOR catalysts for waste tire pyrolysis. The influences of various noble metal-based catalysts on the nature and yield of products, particularly the pyrolytic oil are discussed in relation with the catalyst characterization results.

5.3 Experimental

5.3.1 Catalyst Preparation

Mordenite zeolite (MOR, H-form, SiO2/Al2O3 by mole ratio = 19, BET surface area = 380 m^2/g, purchased from TOSOH, Singapore) was first calcined in air at 500°C for 3 hours. Then, it was loaded with noble metals, Ru (RuCl3, FLUKA), Rh (Rh(NO3)3, ALDRICH), Re (ReCl3, FLUKA), Pt (Pt(NO3)3, FLUKA), using the incipient wetness impregnation technique to obtain 1 wt% each separate noble metal-supported catalysts. After that, the samples were dried in the oven at 110°C for 3 hours followed by calcination in a flow of air at 500°C for 3 hours. Next, they were pelletized, ground, and then sieved to specific particle sizes of 400–425 μm. Prior to catalytic activity measurement, the catalysts were reduced at 400°C by H$_2$ for 3 hours.

5.3.2 Catalyst Characterization

The composition of the prepared catalysts was determined by Inductively Coupled Plasma (ICP) technique using a Perkin Elmer Optima 4300 PV machine after the dissolution of the catalysts using HF solution. The surface area (BET) and pore volume (B.J.H) of the prepared samples were characterized by N$_2$ physical adsorption using the Sorptomatic 2900 equipment. XRD patterns were obtained using the Riguku D/Max 2200H using CuKα small radiation at 40 KV and 30 mA. The catalyst samples were scanned from 5 to 60 degrees (2θ/θ) with a scanning speed of 5°/min.

Hydrogen chemisorption was carried out using a conventional laboratory made-up system equipped with a TCD detector. Prior to performing the chemisorption at room temperature, an approximate 50 mg of reduced sample was pretreated in helium at 150°C for 0.5 hour. Dispersion data was calculated by assuming a stoichiometry H/M =1 [13,19,20]. Temperature-programmed desorption (TPD) using NH3 was conducted in a TPD/TPR Micromeritics 2900 apparatus. Approximately 0.1g of sample was first pretreated in He at 150°C for 30 minutes. Then, the system was cooled to 100°C, and the NH3 adsorption was performed using NH3/N2 for 1.5 hours followed by the introduction of He to remove the physically adsorbed NH3 for 30 minutes at 100°C. Finally, the system was cooled to 50°C, and then the temperature program desorption was started from 50°C to 600°C with a heating rate of 5°C/min. For Temperature-programmed reduction (TPR) using

hydrogen, the calcined sample was heated to 150°C and kept at this temperature for 1 hour under the flow of helium to remove water and other contaminants. TPR profiles were recorded with a temperature program from room temperature to 700°C (10°C/min). TPD-H2 was conducted using the same Micromeritics apparatus. The reduced sample was pretreated under helium flow at 150°C and then cooled to room temperature. H2 adsorption was performed at room temperature for 0.5 hour using UHP H_2 followed by flushing with helium at the same temperature for another 0.5 hour. The H_2-TPD was performed from room temperature to 600°C at a rate of 10°C/min under helium flow. The amount of desorbed hydrogen was monitored by a TCD. Temperature-programmed oxidation (TPO) was performed using the apparatus for TPR from room temperature to 900°C (10°C/min), and the final temperature was held for 30 minutes. The amount of coke was then determined from the area under the curve and calculated by the software equipped with the machine. The sulfur contents in the spent catalysts were determined by X-ray fluorescence (XRF) spectrometer, Philips PW2400.

5.3.3 Pyrolysis of Waste Tire

The detail of pyrolysis process was described elsewhere [9]. Briefly, a tire sample was pyrolyzed in the lower zone of the reactor (500°C), and then the evolved product was carried to the upper zone packed with a catalyst (350°C). The obtained product was next passed through a condensing system to separate incondensable compounds from the liquid product. The solid and liquid products were weighed to determine the product distribution. The amount of gas was then determined by mass balance. The gaseous product was analyzed by a GC equipped with an FID. Prior to being analyzed, the liquid product was dissolved in n-pentane to precipitate asphaltenes. The obtained maltenes was analyzed by liquid adsorption chromatography [24]. Consequently, saturated hydrocarbons, mono-, di-, poly- and polar-aromatics in the maltenes were fractionated. Finally, a SIMDIST GC was used to analyze the obtained maltene and hydrocarbon fractions according to the ASTM D2887 method to determine the simulated true boiling point curves. The curves were then cut into petroleum fractions based on their boiling point, including naphtha (<200°C), kerosene (200°C-250°C), gas oil (250°C – 370°C) and residue (>370°C).

5.4 Results and Discussion

5.4.1 Catalyst Characterization

The amounts of metal loaded on each sample determined by ICP are presented in Table 5.1. Accordingly, the true numbers are very close to the targeted values. Figure 5.1 shows the diffraction patterns of the reduced catalysts and HMOR support. The introduction of metal did not influence the structure of the parent zeolite. And, the peaks corresponding to the metal species are hardly detected, possibly because the amount of metal loaded is below the detectable range of the machine.

Table 5.1 Physical and chemical properties of the studied catalysts

Catalyst	M %wt	Dispersion (%)	Surface area (m^2/g)	Pore volume (cm^3/g)	Asphaltenes (g/g oil)
HMOR	-	-	372.5 ± 9.3	0.23	-
Pt/HMOR	0.94	30.8	359.8	0.20	0.000494
Re/HMOR	0.97	35.4	350.5	0.21	0.000654
Rh/HMOR	1.02	27.3	352.7	0.21	0.000387
Ru/HMOR	0.98	21.1	354.9	0.20	0.000309

Several structure properties of the prepared catalysts obtained from N_2 adsorption/desorption analysis are also shown in Table 5.1. The incorporation of noble metals slightly decreases both surface area and pore volume of the parent zeolite support. And, all the prepared catalysts have comparable surface area and pore volumes.

Metal dispersion determined by H_2-chemisorption is also given in Table 5.1. It can be seen that there exists small difference between the metal dispersion among all the prepared samples. However, the order of metal dispersion can be summarized as followed: Re/HMOR > Pt/HMOR > Rh/HMOR > Ru/HMOR. In addition, the average metallic particle size in all catalysts is in the range of 2.5 nm to 4 nm, which is much larger than the pore diameter of the main channel of HMOR zeolite. This, together with the decrease in both surface area and pore volume of the

parent zeolite after incorporation of metal, suggests the occurrence of pore blockage and/or to a smaller extent, the diffusion of noble metal into the zeolite channels.

The strength and concentration of acid site in the reduced M/HMOR were revealed by TPD of ammonia, and the obtained results are presented in Figure 5.2. In good agreement with the TPD-NH$_3$ studied by [25], the ammonia desorption curve of HMOR shows two desorption peaks. The first one locates at around 200°C, and the second one peaks at around 540°C, which correspond to the weak and strong acid sites, respectively. It is well-known that the presence and distribution of alumina is intimately related to the acidic property of the zeolite. The extra framework alumina and/or alumina in the bound are responsible for the weak acid sites [26,27]. And the concentration of Bronsted acid sites was found to be proportional to the intensity of the low temperature peak of TPD-NH$_3$ profile of zeolite [27], whereas the amount of strong acid sites decreased with the content of framework alumina [28]. Thus, the weaker acid sites are located closer to the surface, whereas the strong acid sites are located in the deepest part of the zeolite structure [19]. From the figure, obviously the incorporation of noble metals leads to a reduction in the intensity of desorption peaks, particularly the peak corresponding to the strong acid sites for all samples. This occurs because a fraction of -OH groups was eliminated by incorporation with the metal salt precursors during catalyst preparation and/or the blockage of metal particles, then decreasing the accessible acid sites, particularly the ones inside the zeolite channels. And, the order of total acid concentration for noble metal-supported catalysts is as follows: Ru/HMOR > Re/HMOR > Rh/HMOR > Pt/HMOR. In the TPD-NH$_3$ spectra of Rh and Pt catalysts, the number of strong acid sites decreases drastically. The TPD-NH$_3$ profile of the Ru/HMOR shows a new peak at the temperature in the range corresponding to weak acid sites with a maximum around 250°C (Figure 5.2). This new peak is attributed to ruthenium clusters, which were reported to have high tendency to adsorb ammonia [12] and/or to have occurred from the interaction between metal and support for Ru-based catalyst [18].

Temperature-programmed reduction is a powerful technique to study the reduction behavior of oxide phases or salts, as well as providing information regarding the degree of interaction between metal and support. Mordenite is comprised of two channel types: (i) larger channel, also called main channel,

accessible through twelve member oxygen rings with an opening of 7.0 Å x 6.5 Å, and (ii) smaller channels, often referred to as side-pockets, which include eight member oxygen rings with 3.4 Å x 4.8 Å [29]. Thus, hydrogen with a kinetic diameter of 0.24 nm can enter the inner zeolite structure, and the reduction of metal oxides/salts may occur somewhere on the zeolite surface, in the zeolite channels, or in the side-pockets [19]. Another important outcome of TPR analysis, therefore, is the location of species in the zeolite. The TPR profiles of all prepared catalysts are shown in Figure 5.3. As expected, the TPR profile of the HMOR zeolite shows no peaks (not included in the figure). The profile of Rh catalyst shows the two overlapping peaks having the maxima at 109°C and 135°C that can be attributed to the reduction of Rh^{3+} in two different environments [30]. These are not necessary to be two different electronic states, but possibly due to Rh_2O_3 having different metal particle sizes, which interact in different ways with the support [30]. A very broad and low intensity peak is also observed at around 360°C in the H_2-consumption curve of Rh-catalyst, suggesting the presence of the other rhodium species in a more difficult reduction environment. The TPR result of Pt/HMOR catalyst shows a unique, very broad peak with a maximum at around 489°C. The broad peak suggests the reduction of platinum species located at different environments. This peak can be ascribed to the reduction of Pt^{2+} located in the main channel and/or the side-pockets in the zeolite [19]. The hydrogen consumption curve of Re catalyst shows a unique, fairly broad peak with a maximum at approximately 370°C. The widening of the peak is possibly due to the reduction of rhenium species located in different environments. The Ru/HMOR exhibits a main peak centered at about 198°C. The very intense peak is possibly due to the reduction of Ru^{3+} uniformly dispersed on the surface of the zeolite [31]. The profile also shows a small and ill-defined band of hydrogen consumption between 350°C and 450°C which could correspond to a small amount of ruthenium oxide or oxychloride formed by the exposition and drying in air during catalyst preparation [12]. It is also worthy mentioned that although the reduction temperatures of Re and Pt supported on HMOR catalysts are, to a certain extent, higher than that used for catalyst reduction during preparation, the complete reduction of all prepared samples was confirmed since the reduced samples did not consume any hydrogen. This effect might be explained by the long reaction time of

reduction employed (3 hours, 400oC).

Figure 5.4 depicts the TPD-H_2 profiles of all prepared catalysts. Accordingly, the profile of the bare zeolite support shows no peak. And all profiles exhibit a unique peak located at temperatures lower than 350°C, corresponding to the desorption of hydrogen that chemically adsorbed on the surface of the metallic particles. Considering the intensity of the peak, which is the indication of the hydrogen adsorption capacity on the metallic sites, the observed trend is: Re > Pt > Ru > Rh. This result is in a good agreement with the H_2-chemisorption analysis. Moreover, based on the desorption temperature, it can reveal that the strongest hydrogen adsorption is observed over Ru/HMOR catalyst.

5.4.2 Pyrolysis Products

5.4.2.1 Product Yields

Figure 5.5 shows the product distribution, i.e. the yield of gas and liquid product. For the non-catalytic pyrolysis, the yields (%wt) of solid, liquid and gas are approximately 47%, 42% and 11%, respectively. The solid product is mainly carbonaceous material and therefore, as expected, the yield of solid obtained from all runs is similar (not shown in the figure). This is attributed to the fact that the pyrolysis conditions were kept constant and the tire is completely decomposed at 500°C [9].

The presence of catalysts strongly influences the yield of gas and liquid products. Except Re, the incorporation of noble metals drastically increases the yield of gas product at the expense of liquid yield and the order of gas production is: Ru > Pt > Rh > Re. The increment of gaseous product can be attributed to the cracking activity of the studied catalysts. The presence of metallic clusters might further promote cracking reactions over acid sites by initially hydrogenating the unsaturated compounds [11] due to their high hydrogenation activity [19,20]. As a consequence, a higher amount of HCs were cracked into lighter compounds, resulting in the increase in the yield of gas product. The high activity of the noble metal-supported catalysts also leads to a drastic asphaltenes reduction, as shown in Table 5.1.

5.4.2.2 Petroleum Cuts

The influences of various noble metal-based catalysts on the

petroleum cuts of the derived oils are illustrated in Figure 5.6. It can be seen that the bifunctional catalysts with various metals strongly influence the contents of petroleum fractions in the oils. In the non-catalytic oil, although the content of naphtha is the highest (~30%) among other petroleum fractions, but there still exists a high portion of in the heavy fractions that can be cracked further to naphtha. The treatment of noble metal-supported catalyst leads to a shift of hydrocarbons from heavy fractions toward lighter fractions, particularly naphtha, indicating that lighter oils were produced. The high activity of noble metal-supported catalysts for light oil production, again, can be attributed to their bifunctionalities, which is further discussed in Section 3.4. In general, the order of naphtha production (Figure 5.6) for different metals is as follow: Ru > Pt > Rh > Re. This order is similar to the order of gas production (Figure 5.5). However, it should be noted that the activity on naphtha production of Re/HMOR is lower than the bare HMOR support.

5.4.2.3 Composition of Pyrolysis Oil

The oil obtained from non-catalytic pyrolysis contains a high concentration of aromatic hydrocarbons, particularly the high content of polar-aromatics (~12%wt). Noble metal-supported catalysts significantly affect the compositions of the derived oils, as shown in Figure 5.7. It can be seen that the contents of saturates and single ring aromatics increase in accordance with the reduction in both multi ring aromatic compounds, i.e. di- and poly-aromatics, and polar-aromatics. Moreover, it should be noted that the reduction in poly- and polar-aromatics is more pronounced as compared to the reduction in di-aromatics for all studied catalysts. And the highest activity for aromatic reduction is observed over Ru-based catalyst, meaning that its oil has the highest concentration of saturates, whereas the oil produced over Re/HMOR has the highest concentration of aromatic hydrocarbons. The content of different types of hydrocarbon in oils generated over Rh- and Pt-based catalysts can be comparable. However, the Pt-supported catalyst produces slightly higher saturates and lower di-aromatics than the Rh one.

5.4.3 Discussion

5.3.4.1 Activity

The complex structure of tire makes it difficult to understand the multi-reactions occurring during pyrolysis. And, aromatics are produced and

consumed during the catalytic pyrolysis of waste tire through different reactions, such as Diels-Alders reaction, aromatization, condensation, dealkylation, hydrogenation, cracking, etc [4,9,32]. As reported in our previous paper, the use of HMOR decreased the poly- and polar-aromatics content in the derived oil [9]. And compared to the bare zeolite support, the incorporation of noble metal to the zeolite leads to a further reduction in the concentration of multi-ring aromatic compounds as well as polar-aromatics, except for Re/HMOR (Figure 5.7).

Table 5.2 summarizes the kinetic diameters of several aromatics [33]. As such, the main channel of the zeolite support is not accessible for the poly-aromatics but for di-aromatics to a small extent.

Table 5.2 The kinetic diameters of several aromatics [33]

Compound	H/C atomic ratio	Boiling point (^{o}C)	Molecular size (Å)
Alkylbenzenes	1.0-1.4	200-250	5 x 6.8
Naphthalene	1.26	218	6x7
Tetrahydronaphthalene	1.38	206	6 x 7
Anthracene	0.94	340	6 x 9.5
Pyrene	0.63	404	8.5 x 8.5

As observed from the H_2-chemisorption analysis and TPR profiles, a considerable amount of noble metal particles locates outside the zeolite structure. Moreover, there is a high density of weak sites that are probably located at the outer surface of HMOR zeolite. And the amount of weak acid sites accounts for a high portion of the total acid sites in the prepared bifunctional catalysts. Therefore, on the outer surface of the zeolite support there presents a considerable concentration of both metallic and acidic sites that are accessible for the di-, poly- and polar-aromatics trying to enter the zeolite channels. Accordingly, the multi-ring aromatics produced from tire cracking might be hydrogenated over metallic sites, producing (partial) hydrogenated compounds, which rapidly undergo cracking and/or ring-opening on the acid sites [34]. As a consequence, noble metal can promote the conversion of the heavy compounds like multi-ring aromatic and polar-aromatics to the lighters; thus,

producing lighter oil (Figure 5.7) and the oil contains higher concentration of saturates (Figure 5.6). The presence of noble metal has another advantage in that it can prevent a new formation of the polar- and poly-aromatics [32]. Furthermore, the higher reduction of poly-aromatics than di-aromatics can be ascribed to their higher reactivity to hydrogenate [35]. However, the high amount of coke (Table 5.3), which could be produced by the condensation of the polycyclic aromatics [9] and polar-aromatics [32], might be also responsible for the reduction of poly- and polar-aromatics in oil to a small extent.

On the other hand, it is well accepted that the metal dispersion influences the hydrogenation activity of noble metal-supported catalysts [30]. In this paper, the order of metal dispersion for the prepared catalysts as revealed from H_2-chemisorption analysis is: Re > Pt > Rh > Ru. Moreover, it has been reported that the cracking reactions over acid sites are dominant compared with hydrogenolysis over metal sites [19]. For the current catalysts, the order of total concentration of acid sites as revealed from TPD-NH_3 analysis is: Ru > Re > Rh > Pt. The catalyst activity in terms of the multi-ring aromatic reduction and light oil production is in the following order: Ru > Pt > Rh > Re. One can see that this order does not match with that of the metal dispersion or acidity. Therefore, it is safe to conclude that the nature of noble metals strongly influences the catalytic activity of the noble metal supported on HMOR catalysts.

5.3.4.2 Coking and Sulfur Poisoning

The amounts of coke on the spent catalysts determined by TPO analysis are given in Table 5.3.

Table 5.3 Coke and sulfur in the spent catalysts

	Ru/HMOR	Rh/HMOR	Pt/HMOR	Re/HMOR
Coke (wt%)	16.4	20.8	21.3	29.7
S (wt%)	0.78	1.21	1.35	2.51

Generally, the order of the amount of coke on the spent catalysts is: Re > Rh > Pt > Ru. It is noted that due to the intrinsic structure of HMOR zeolite that has one main

channel, once one segment of the channel is block, the whole channel is rendered inactive. Liquid analysis reveals a considerable amount of polar-aromatics (Figure 5.7), which are mainly sulfur-containing aromatics [32]. And these sulfur containing compounds can poison the metal sites by the strong bonding between the sulfur atoms and metal atoms [12,36], making the metal sites inactive, and consequently favoring coke formation. Therefore, the sulfur contents in all the spent catalysts were analyzed by XRF, and the obtained results are also summarized in Table 5.3. Accordingly, the order of sulfur content in these samples is: Re > Pt > Rh > Ru. From these results, it is safe to conclude that Ru/HMOR exhibits both the highest sulfur-tolerance and the lowest coke formation.

The extent and strength of adsorption of a sulfur containing polar-aromatic on a metal site depend mainly on: (i) the electron-donor character of the compound; and (ii) the electronic structure of the metal [37]. The intrinsic characteristic of electronic structure of the metal can be represented by its local density of unoccupied states at the Fermi level, $N(E_F)$ [30]. This density of state indicates the number of quantum states of a metal that is available for its bonding with reactants. So, the lower the $N(E_F)$ of a metal is, the more difficult it is to adsorb a molecule [38]. However, the values of $N(E_F)$ are not easily available; thus, we used the metal electronic heat capacity C_{el}, which depends directly on $N(E_F)$ [39]:

$$C_{el} = (\pi^2/3)\, N(E_F)\, k_B^2\, T = \gamma\, T \qquad (1)$$

where k_B is Boltzmann constant, T is absolute temperature and γ is the heat capacity constant of metal. The values of γ for different metals are given in Table 5.4.

Table 5.4 The metal heat capacity constant (γ) [39]

	Ru	Rh	Pt	Re
γ (mJ/mole.K^2)	3.3	4.9	6.8	2.3

According to the values of γ in Table 5.4, the order of sulfur tolerance should be: Re/HMOR > Ru/HMOR > Rh/HMOR > Pt/HRMO. Without taking Re/HMOR into account, this order is exactly the same as what we have experimentally found for both the amount of coke and the sulfur content in the spent catalysts (Table 5.3). Additionally, the sulfur tolerance of metal-supported catalyst can be enhanced by the

interaction of the metal with the Bronsted acid sites of the zeolite support, leading to the formation of $M^{\delta+}$, and consequently lowering the strength of the S-M bonds [40]. As such, the highest acidity of Ru/HMOR catalyst might also contribute to its highest sulfur tolerance to a certain extent.

The exceptional case of Re/HMOR can be consciously explained by taking into account the fact that the intrinsic nature of Re was shown to be catalytically inactive for hydrogenating reaction [21]. It is known that when the metallic function has no proper hydrogenation activity, the unsaturated bonds can not react quickly enough. Therefore, when the acid sites generate alkenes and aromatics from β-scission and aromatization (cyclization and subsequent hydride transfer), respectively [19], these unsaturated compounds can not be hydrogenated as fast as possible, leading to the consequent formation of aromatic compounds. Furthermore, the high temperature used in this study is, to a certain extent, responsible for favorable aromatization. Consequently, the condensation of aromatics, including sulfur-containing polar-aromatics might be promoted, leading to the high amount of coke as well as sulfur in the spent catalyst. That explains the low activity of Re/HMOR catalyst, even lower than the bare HMOR zeolite support in the present study (Figures 5.5-5.7).

5.5 Conclusions

The uses of noble metals (Rh, Re, Ru, Pt) supported on HMOR catalysts produced an important increase in the yield of gaseous product at the expense of the oil yield. This effect was attributed to the high activity of the bifunctional catalysts for the conversion of polycyclic and polar-aromatic hydrocarbons into lighter compounds. And the aromatic reduction is more pronounced for poly- and polar-aromatics than for di-aromatics. The polycyclic and polar-aromatic reduction and simultaneously light oil production activities for the current catalysts can be summarized in the order: Ru/HMOR > Rh/HMOR > Pt/HMOR >> Re/HMOR. We found that these activities were independent on the metal dispersion as well as the total acid concentration, but depend on the intrinsic nature of the noble metal used. The best catalytic performance of ruthenium catalyst was ascribed to its metallic

nature that exhibited highest coke resistance and high hydrogenation activity.

5.6 Acknowledgements

5.7 References

[1]. M.M. Barbooti, T.J. Mohamed, A.A. Hussain, F.O. Abas, J. Anal. Appl. Pyrol. 72 (2004) 165-170

[2]. C. Berrueco, E. Esperanza, F.J. Mastal, J. Ceamanos, P. Garcia-Baicaicoa, J. Anal. Appl. Pyrol. 74 (2005) 245-253

[3]. E. Aylon, R. Murillo, A. Fernandez-Colino, A. Aranda, T. Garcia, M.S. Callen, A.M. Mashal, J. Anal. Appl. Pyrol. 79 (2007) 210-214

[4]. Paul T. Williams and David T. Taylor, Fuel 72 (1993) 1469-147

[5]. B. Benallal, C. Roy, H. Pakdel, S. Chabot, M.A. Poirier, Fuel 74 (1995) 1589-1594

[6]. A.M. Cunliffe, P.T. Williams, J. Anal. Appl. Pyrol. 44 (1998) 131-152

[7]. P.T. Williams, R.P. Bottrill, Fuel 74 (1995) 736-742

[8]. S. Murugan, M.C. Ramaswamy, G. Nagarajan Fuel Proces. Techno. 90 (2009) 67-74

[9]. N.A. Dũng, A. Mhodmonthin, S. Wongkasemjit, and S. Jitkarnka, J. Anal. Appl. Pyro. 85 (2009) 338-344

[10]. A. Lugstein, A. Jentys, H. Vinek, Appl. Catal. A: Gen. 176 (1999) 119-128

[11]. M.A. Ali, T. Kimura, Y. Suzuki, M.A. Al-Saleh, H. Hamid, T. Inui, Appl. Catal. A: Gen. 277 (2002) 63-72

[12]. D. Eliche-Quesada, J.M. Meria-Robles, E. Rodriguez-Castellon, A. Jimenez-Lopez, Appl. Catal. B: Environ. 65 (2006) 118-126

[13]. D. Eliche-Quesada, M.I. Macias-Ortiz, J.Jimenez-Jimenez, E. Rodriguez-

Castellon, A. Jimenez-Lopez, J. Mole. Catal. A: Chemical 225 (2006) 41-48

[14]. J.B. McKinley, In: Emett PH, editor. Catalysis, vol. 5. Nework: Reinhold, 1957;

[15]. T.A. Pecoraro and R.R. Chianelli, J. Catal. 67 (1981) 430-445

[16]. J. Barbier, E. Lamy-Pitara, P. Maracot, J.P. Boitiaux, J. Cosyns, F. Verna, Adv. Catal. 37 (1990) 279-318

[17]. J.K. Lee, H.K. Rhee, J. Catal. 177 (1998) 208-216

[18]. V.M. Akhmedov, S.H. Al-Khowaiter, Appl. Catal. A: Gen. 197 (2000) 201-212

[19]. P. Castano, B. Pawelec, J.L.G. Fierro, J.M. Arandes, J. Bilbao, Appl. Catal. A: Gen. 315 (2006) 101-113

[20]. S. Albertazzi, R. Ganzerla, C. Gobbi, J. Lenarda, M. Mandreoili, E. Salatelli, P. Savini, L. Storaro, A. Vaccari, J. Mole. Catal. A: Chemical 200 (2003) 261-270.

[21]. A.K. Aboul-Cheit, S.M. Aboul-Fotouch, N.A.K. About-Gheit, Appl. Catal. A: Gen. 283 (2005) 157-164

[22]. K. Changmin, G.A. Somorjai, J. Catal. 134 (1992) 179-185

[23]. J. Quartararo, S. Mignard, and S. Kasztelan J.Catal.192 (2000) 307-315

[24]. G. Sebor, J. Blaz ek, M.F. Nemer, J. Chromatogr A, 847 (1999), 323-330

[25]. N. Labhsetwar, H. Minmino, M. Mukherjee, T. Mitsuhashi, S. Rayalu, M. Dhakad, H. Haneda, J. Subrt, S. Devotta, J. Mole. Catal. A: Gen. 261 (2007) 213-217.

[26]. E.D. Derouane, J.P. Bilson, Z. Gabelica, C. Mousty-Desbuquoit, J. Verbis, J. Catal. 71 (1981) 447-448;

[27]. F. Lonyi and J. Valyon, Micro. Meso. Mater. 47 (2001)293-301

[28]. L.O. Almanza, T. Narbeshuber, P. d'Araujo, C. Naccache, Y.B. Taarit, Appl. Catal. A: Gen. 178 (1999)39-47.

[29]. J.L. de Macedo, S.C.L. Dias, J.A. Dias, Micro. Meso. Mater. 72 (2004) 119 – 125.

[30]. D. Eliche-Quesada, M.M. Merida-Robles, E. Rodringuez-Castellon, A. Jimenez-Lopez, Appl. Catal. A: Gen. 279 (2005) 209-221.

[31]. D. Eliche-Quesada, E. Rodringuez-Castellon, A. Jimenez-Lopez, Micro. Meso. Mater. 99 (2007) 268-278

[32]. N.A. Dũng, S. Wongkasemjit, S. Jitkarnka, Effects of pyrolysis temperature and Pt-loaded catalysts on polar-aromatic content in the tire-derived oil, Appl. Catal. B: Environ. In Press DOI:10.1016/j.apcatb.2009.05.038

[33]. Tseng-Chang Tsai, Appl. Catal. A: Gen. 301 (2006) 292-298

[34]. N.A. Dũng, S. Wongkasemjit, S. Jitkarnka "Influences of catalyst temperatures and Ru-loaded MCM-41 on waste tire pyrolysis and its products", Manuscript submitted to Journal of Analytical and Applied Pyrolysis.

[35]. A. Corma, A. Martinez, and V. Martinez-Soria, J. Catal. 169 (1997) 480-489

[36]. C. Naccache, M. Primet, M.V. Mathieu, J. Catal. 121 (1973) 266

[37]. A. Arcoya, A. Cortes, J.L.G. Fierro, and X.L. Seoane in C.H. Bartholomew and J.B. Butt (Editors), Catalyst Deactivation 1991, Elservier Science Publishers B.V., Amsterdam

[38]. P.A.Cox, The Electronic Structure and Chemistry of Solids, Oxfort University Press, Oxford, 1987, Ch.3.

[39]. C. Kittel, Introduction to Solid State Physics, 7th Edition, J. Wiley, NewYork, 1984, Ch. 6

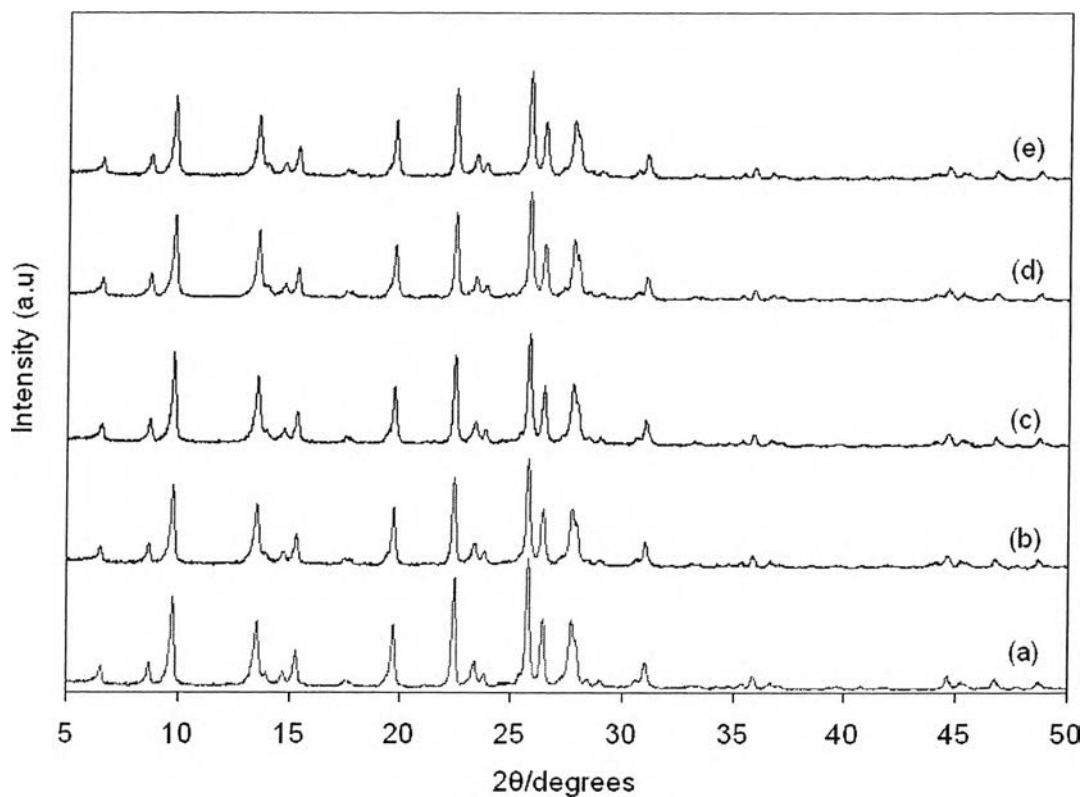[40]. A.M. Venezia, V. La Rarola, B. Pawelec, J.L.G. Fierro, Appl. Catal. A: Gen. 264 (2004) 43-51

Figure 5.1 XRD patterns of (a) HMOR, (b) Ru/HMOR, (c) Rh/HMOR, (d) Re/HMOR, and (e) Pt/HMOR.
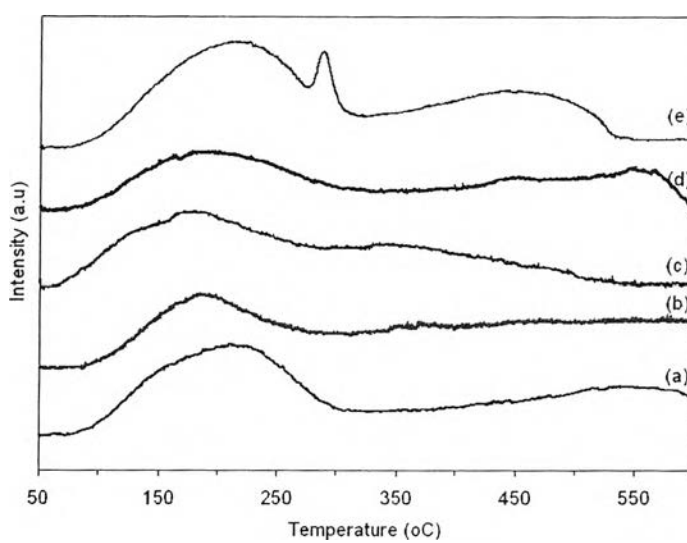

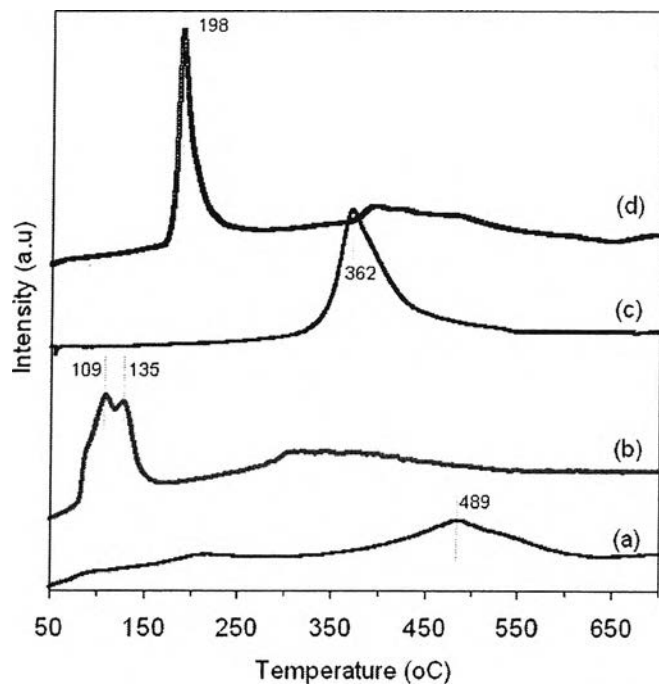**Figure 5.2** TPD-NH$_3$ profiles of (a) HMOR, (b) Pt/HMOR, (c) Rh/HMOR, (d) Re/HMOR, and (e) Ru/HMOR.

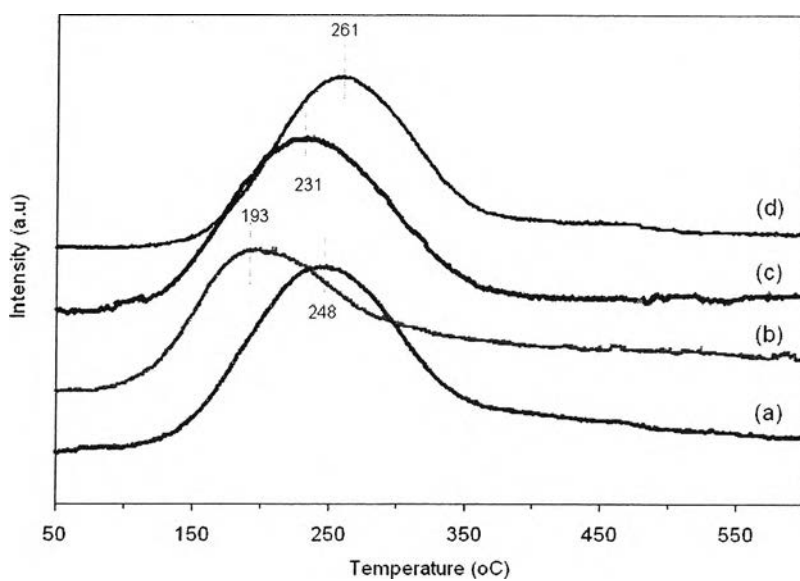**Figure 5.3** TPR-H$_2$ profiles of (a) Pt/HMOR, (b) Rh/HMOR, (c) Re/HMOR, and (d) Ru/HMOR.

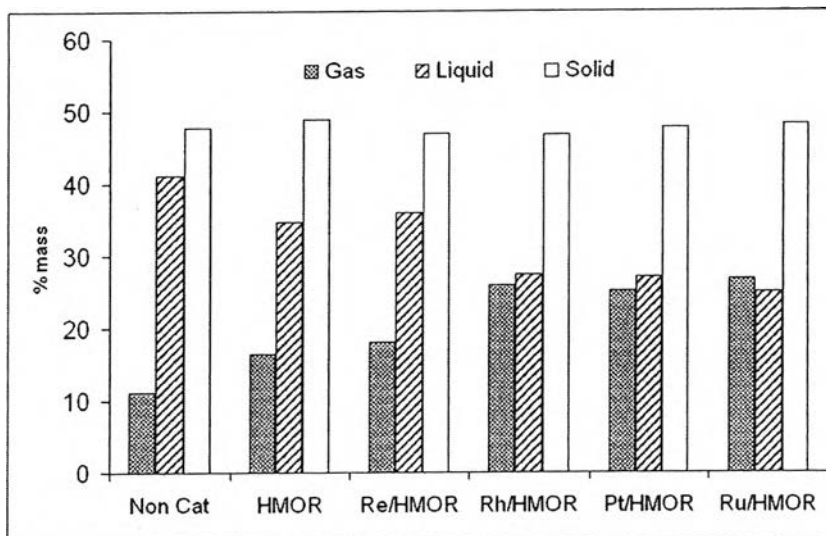**Figure 5.4** TPD-H$_2$ profiles of (a) Pt/HMOR, (b) Rh/HMOR, (c) Re/HMOR, and (d) Ru/HMOR.

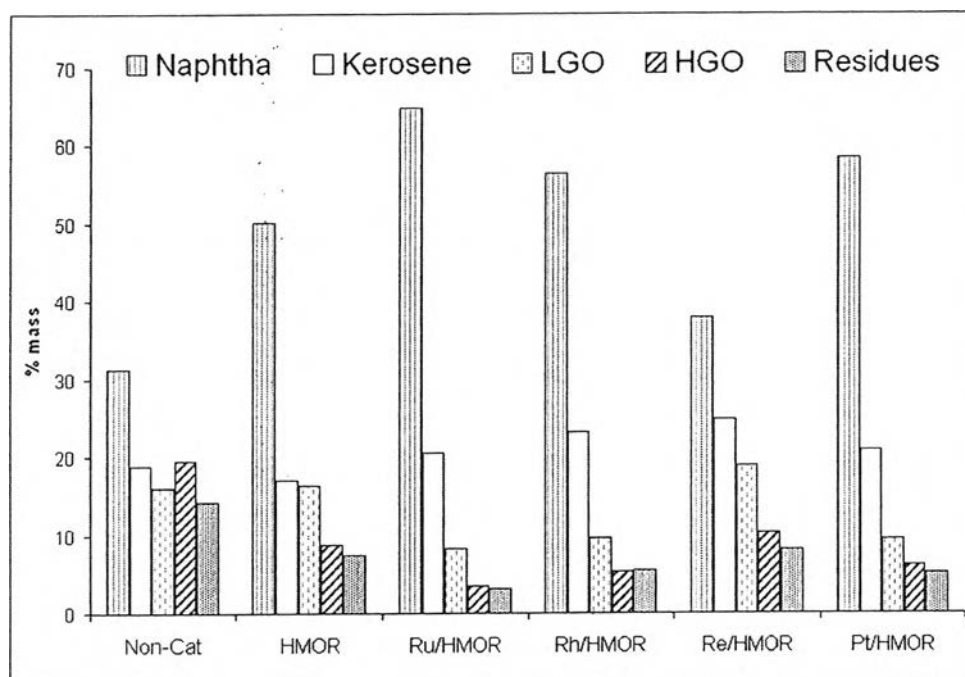**Figure 5.5** Yield (%wt) of pyrolysis products

Figure 5.6 Petroleum fractions of pyrolysis oils obtained from using various catalysts.
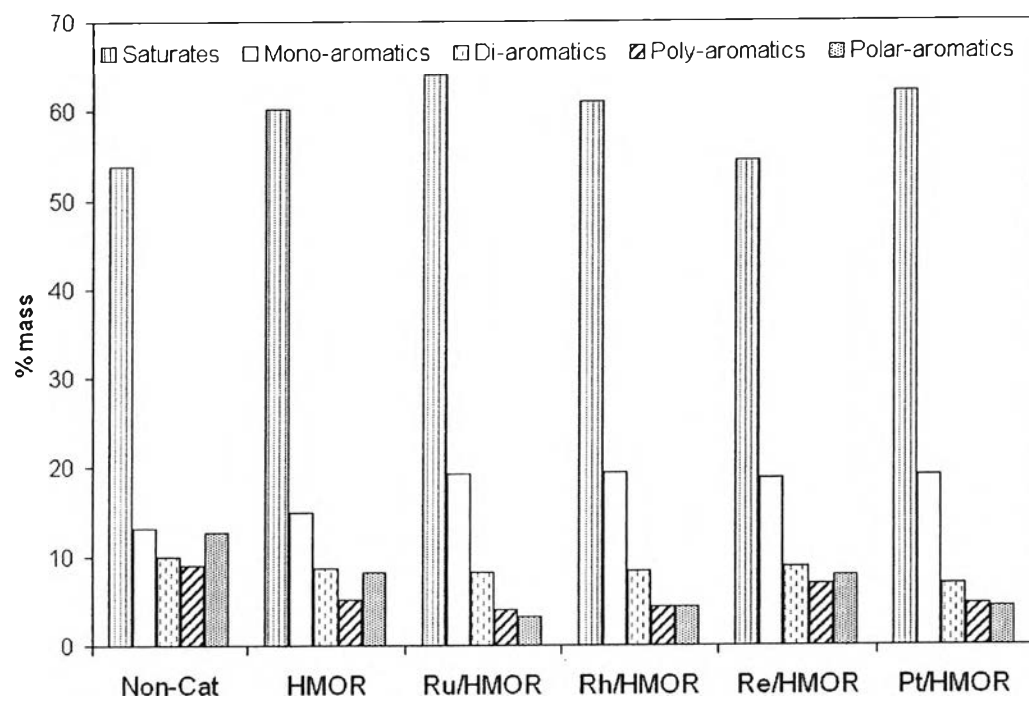
Figure 5.7 Compositions of pyrolysis oils obtained from using various catalysts.